PERFORMANCE OF POWDER-FILLED EVACUATED INSULATION VS. CONVENTIONAL INSULATION IN A SINGLE-WIDE MANUFACTURED HOME UNIT

T.W. Petrie **Jan Kosny** **P.W. Childs**

Jeffrey E. Christian **R.S. Graves**

ABSTRACT

A full-scale section of half the top of a single-wide manufactured home, including part of the side wall, has been studied in a large-scale climate simulator (LSCS) at a national laboratory. A small roof cavity with little room for insulation at the eaves is often the case with single-wide units and limits practical ways to improve thermal performance. The authors wanted to see if superinsulation improved the thermal performance of these units, so the steady-state performance of the roof cavity of the single-wide manufactured home test section was measured when the roof cavity was insulated with fiberglass batt insulation or combinations of batt insulation and powder-filled evacuated panel (PEP) superinsulation. Three insulation configurations were tested: A, a base-case configuration with two layers of nominal R_{US} - 7 $h \cdot ft^2 \cdot °F/Btu$ (R_{SI} - 1.2 $m^2 \cdot K/W$) fiberglass batts; B, superinsulation with a layer of PEPs and one layer of the fiberglass batts; and C, four layers of the fiberglass batts. Configurations A and B were also modeled to get detailed insight into the performance of the superinsulation and base-case insulation systems.

Center-of-cavity R-values and system R-values for the whole test section showed the effects of certain features of the systems. The high R-value PEPs fit easily between the trusses but did not cover the ceiling joists. The lengths of the PEPs were such that it took three panels between each pair of joists to span the distance from eave to ridge; the joints were underinsulated. The configurations with only fiberglass batts had significant compression of insulation at the eave edge of the test section; the one with PEPs did not. All configurations left the eave edge underinsulated relative to the center-of-cavity R-value.

Results under winter conditions were as follows:

Configuration	*Center of Cavity R_{US} (R_{SI})*	*System R_{US} (R_{SI})*	*System/ Center (%)*
A. Two Layers FG Batts	*15.6-17.2 (2.7-3.0)*	*12.0-12.4 (2.1-2.2)*	*72-77*
B. PEP + One Layer FG	*24.0-25.8 (4.2-4.5)*	*12.4-12.7 (about 2.2)*	*49-53*
C. Four Layers FG Batts	*30.4-31.7 (5.4-5.6)*	*16.8-18.6 (3.0-3.3)*	*55-59*

The tests of the fiberglass batt configurations at summer conditions showed slightly lower center-of-cavity R-values and higher ratios. The configuration with PEPs was not tested at summer conditions. Additional tests with sheathing that covered underinsulated areas and modeling with a three-dimensional conduction program showed that the lower percentage of system to center-of-cavity R-values for the configuration with PEPs was due to joist and joint effects as well as the effects of the horizontal thermal bridge at the eave edge. The four layers of fiberglass batts showed mainly the effects of compression of insulation at the eave edge. Models of the two-layer fiberglass batt and the PEP insulation systems predicted that 16% of the total heat flow through the system area was due to the eave edge alone. For these models, the eave edge comprised the side wall of the test section and enough ceiling to include the region where the two layers of fiberglass batts were compressed between the roof and ceiling—only 8.4% of the system area.

INTRODUCTION

A roof test section was built that represented half of the top of a single-wide manufactured home. It was designed to permit testing of different roof cavity insulations in a large-scale climate simulator (LSCS) at a national laboratory. The LSCS allows temperatures to be established above test sections that simulate outdoor conditions ranging from extreme winter to extreme summer climates. Corresponding indoor conditions are established below the test sections. For this work, only steady-state tests were run.

The purpose of the tests was to obtain comparative thermal performance data for the roof cavity of the single-wide manufactured home test section when the roof cavity was insulated with fiberglass batt insulation or

T.W. Petrie, Jan Kosny, P.W. Childs, Jeffrey E. Christian, and **R.S. Graves** are with the Buildings Technology Center at Oak Ridge National Laboratory, Oak Ridge, Tenn.

combinations of batt insulation and powder-filled evacuated panel (PEP) superinsulation. Three insulation configurations were tested: a base-case configuration with two layers of nominal R_{US} - 7 h·ft²·°F/Btu (R_{SI} - 1.2 m²·K/W) fiberglass batts, superinsulation with a layer of PEPs and one layer of the fiberglass batts, and four layers of the fiberglass batts. The thermal performance with the superinsulation configuration and the four layers of batts compared to that with the base case documents how much improvement can be made without changes in construction techniques or appearance of manufactured housing

This series of tests is another use of the LSCS to study and enhance the thermal behavior of full-size features of commercial and residential roof systems. Previous studies documented the thermal performance of several commercial roofing systems side by side (Courville et al. 1989), large reflective air spaces (Petrie et al. 1989), low-slope roofing systems in which there was moisture movement (Pedersen et al. 1992), and residential attic insulation systems (Wilkes et al. 1991a, 199lb; Wilkes and Childs 1992). Modeling of the results by heat and mass transfer programs is an essential part of the procedures to analyze data obtained in the LSCS. The program used in the present study (Childs 1993) is useful for calculating multidimensional heat flows through components of building envelopes (Kosny and Christian 1995a, 1995b).

TEST SECTION AND INSTRUMENTATION

Figures 1a and 1b are photographs of the test section before and after installation of instrumentation, guard insulation, and the PEPs on top of a layer of fiberglass batts. The overall length of the test section is 12.5 ft (3.8 m) and the height is 2.7 ft (0.83 m), but the roof trusses are only 6.8 ft (2.1 m) wide, corresponding to the width of half the roof of a 14-ft (4.3-m) single-wide manufactured home. LSCS diagnostic platforms for holding test sections require a 12.5 ft (3.8 m) square test section. Extensions to the width were made from oriented strand board (OSB), and the test section rested on 0.75 in. (1.9 cm) thick extruded polystyrene (XPS) foam insulation strips in a diagnostic platform. For detailed sizes of components of the test section, including construction drawings, see Petrie et al. (1995).

The manufactured home test section was built by a Tennessee manufacturer with materials and tools used in regular production. Standard trusses for a 14 ft (4.3 m) wide production model with a flat ceiling were cut in half for the test section. The only significant deviation from actual construction practice was to allow the sheet metal roof to be removable for installing and checking instrumentation and changing insulation configurations. Guard insulation seen in Figure 1b on all four sides of the test section and instrumentation were installed by personnel at the national laboratory.

Figure 1c shows a sketch of the manufactured home test section in the LSCS, with special emphasis on the thick guard insulation at the ridge edge and part of the eave edge. The test section was designed so the total heat loss or gain through an 8-ft (2.4-m) length of the entire ceiling and the 2.5 in. (6.4 cm) of side wall above the guard insulation on the eave edge flowed through the nominal 8-ft by 8-ft (2.4-m by 2.4-m) opening of the metering chamber of the LSCS. The energy balance on the metering chamber, which yields the net energy flow through the specimen, was checked for systematic error as part of the tests. A featureless panel comprising 4.0 in. (10.2 cm) of expanded polystyrene, having a known R-value of about 16 h·ft²·°F/Btu (2.8 m²·K/W), was inserted as a calibration test panel after most of the tests with the manufactured home test section had been completed. The metering chamber balance and temperatures measured on the top and bottom of the known area of the calibration panel reproduced its known R-value within ±0.1 h·ft²·°F /Btu (±0.02 m²·K/W) at winter conditions and, for a fixed amount of cooling by the chilled-water loop in the metering chamber, within ±0.3 h·ft²·°F/Btu (±0.06 m²·K/W) at summer conditions. The success of this check indicates that there is no significant systematic error in the energy balance on the metering chamber, since the operating conditions in all chambers were varied over the same ranges and in the same manner for the calibration panel and the manufactured home test section.

The manufactured home test section was designed to represent a metal-roofed, single-wide manufactured home. Two features at the eave edge of the roof of this type of manufactured home reduce thermal performance: the 0.375 in. (9.5 mm) thick gypsum ceiling extends over the top plate of the side walls, and the short 2.5-in. (6.4-cm) heel leaves little space for insulation at the eaves. Consequently, at the eave edge of the roof there are areas with reduced insulation in the vertical direction and thermal bridges in the horizontal direction. Figure 1c shows that, due to the wall at the eave edge, these areas affect the metering chamber energy balance, which is desired. However, there are also areas at the ridge edge and at the ends along the length that affect the energy balance. These flanking losses are not due to features of the roof of a real manufactured home.

At the eave edge, the test section was built on an 8.6 in. (22 cm) high wall that had drywall on the inside, aluminum siding on the outside, and was fully insulated between nominal 2-in. by 4-in. (actual 38-mm by 89-mm) studs located 16 in. (41 cm) on center (o.c.). This wall has a flat 2-in. by 4-in. (actual 38-mm by 89-mm) top plate. The 0.375 in. (0.95 cm) thick gypsum ceiling and polyethylene air barrier/vapor retarder over it extended to the outside edge of the top plate. During the tests, only 2.5 in. (6.4 cm) of eave wall were exposed to outdoor climatic conditions. The remaining 6.125 in. (15.6 cm) of this wall were insulated with a slab of expanded polystyrene (EPS) insulation, as seen in Figure 1c. The slab of EPS insulation rested on top of a 0.625 in. (1.6 cm) thick piece of OSB and both extended to the edge of the diagnostic platform. The

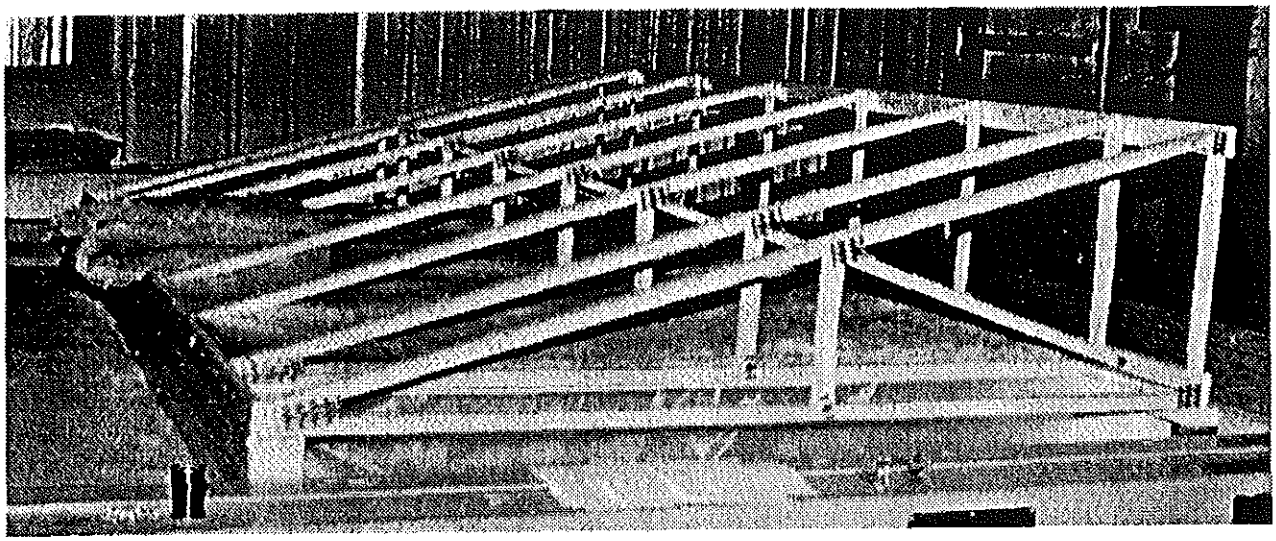

a. Before

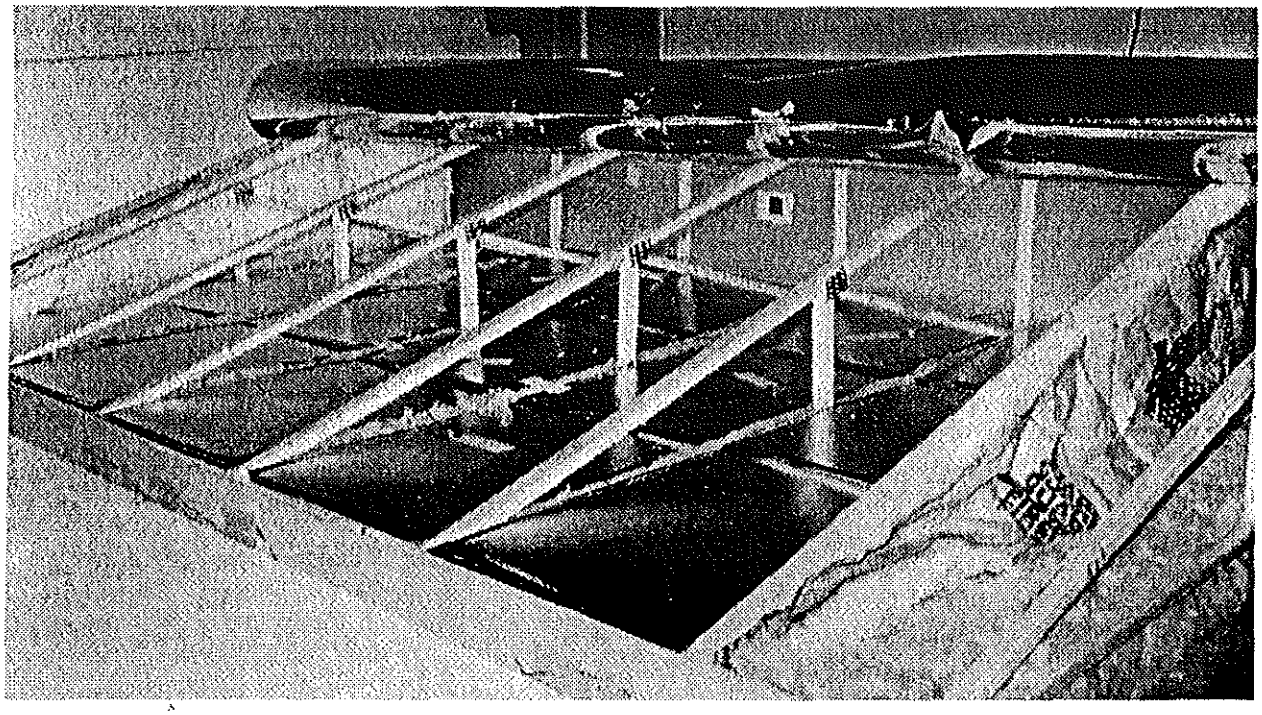

b. After

Figure 1a and 1b *Photographs of the test section before and after installation of instrumentation, guard insulation, and the PEPs on top of fiberglass batt insulation.*

inside edge of the eave wall was in line with the inside edge of the metering chamber wall.

Heat flows through all interior surfaces of the test section except the ceiling and wall at the eave edge are flanking losses. The metering chamber energy balance was corrected for them by calculating or measuring them and subtracting them from the total measured energy flow into the metering chamber. There were four such surfaces. Two were at the ridge edge, where the width of the half-roof of a 14 ft (4.3 m) wide manufactured home was 19 in. (48 cm) short of extending to the other side of the metering chamber. Another wall, like the eave wall except for no aluminum siding, was built there for support of the roof trusses. A heat flux transducer (HFT) was placed in the middle of its area and was assumed to measure the average heat flux for the wall. After enough experiments to include all the

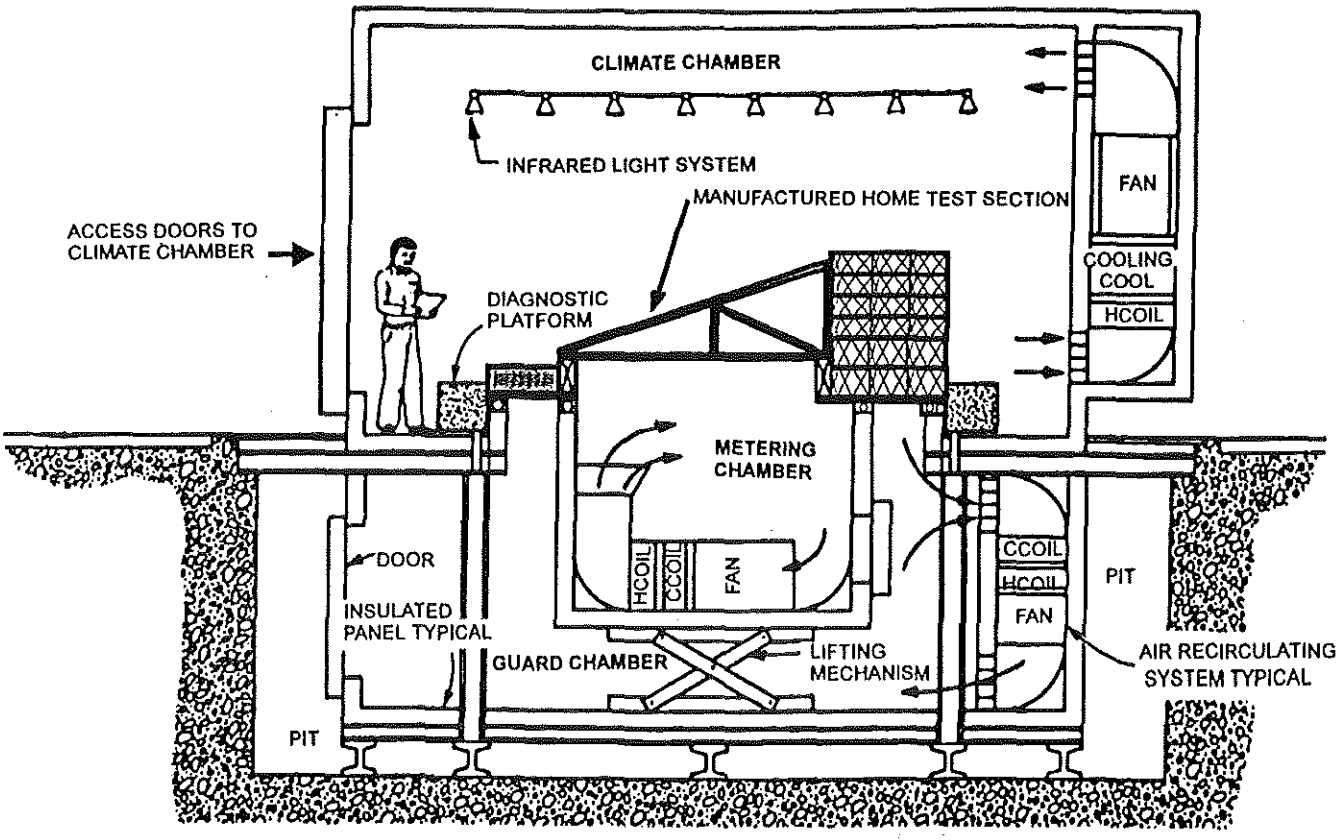

Figure 1c *Schematic of the manufactured home test section inside the large-scale climate simulator.*

different climate chamber temperatures, the HFT was covered by a 6-in. (15-cm) square of 0.5 in. (1.3 cm) thick extruded polystyrene (XPS). The HFT was calibrated facing a 2-ft (0.66-m) square of the same XPS to fit in a heat flowmeter (ASTM 1991). The response of the HFT covered by XPS was applied to a unit area of bare wall by multiplying its indicated heat flux by the ratio of thermal resistances of the wall with the XPS and without it.

Also at the ridge edge, a piece of OSB extended horizontally from the bottom of the ridge wall to the edge of the diagnostic platform. Part of it was exposed to the metering chamber. The top of the OSB was covered by EPS insulation that extended several inches above the peak of the trusses. The total R-value of this EPS in the vertical direction is estimated to be 144 $h \cdot ft^2 \cdot °F/Btu$ (25 $m^2 \cdot K/W$). A one-dimensional estimate of the heat exchange with the metering chamber vertically through the exposed area of OSB was obtained by using this R-value and measured temperatures in the climate chamber and metering chamber.

A steady-state two-dimensional conductive heat transfer calculation was performed at all climate chamber temperatures to estimate the flanking losses through the wall at the ridge edge and vertically through the OSB. The two-dimensional calculation for the wall gave 0.9% to 1.0% of the total measured flow vs. 2.1% to 3.2% from the HFT. The two-dimensional calculation of the flanking loss in the vertical direction was 2.5% to 2.8% vs. 1.7% to 2.0% by the one-dimensional approach. The results from the HFT and from the one-dimensional estimate were used to correct the energy balance.

The remaining two surfaces where flanking losses occurred were along the length of the test section. End walls were built from OSB and extended from the ceiling of the test section to the inside edges of the metering chamber walls. Caulk around them prevented the direct exchange of air between the guard and the metering chambers. Additional pieces of OSB extended horizontally from the bottoms of these end walls to the edges of the diagnostic platform. They created dead air spaces for 1 ft (0.3 m) outside both end walls. The spaces were eventually filled with unfaced fiberglass batt insulation. Each end wall also had a calibrated HFT in the middle of it whose response was used to give each one's flanking loss by following the same procedure as for the HFT on the ridge wall. The heat flow through each wall proved to be about 4% of the measured total before the dead air spaces were filled with insulation and 2% to 3% afterward.

Any flanking loss through the EPS on the eave edge was not deducted from the metering chamber energy balance. Thus, all the heat flow through the eave wall was included in the energy balance. Modeling of heat flow through the eave edge, which was done as part of the data analysis, also included the heat flow through all of the wall at the eave edge. The EPS at this edge was included as a component in the model. One more correction was made to the energy balance besides the four flanking losses. As

in a standard guarded hot box method (ASTM 1989), measurements of temperatures on the inside and outside of the metering chamber walls, along with the known R-value of the walls, allowed correction for the very small heat exchange between the guard and metering chambers.

The boundaries for heat flow between the test section and the metering chamber are taken at the inner edges of the metering chamber walls along the inside surfaces of the OSB end walls and the gypsum eave and ridge walls. That is, the area on which, for example, system R-value is based is the sum of the ceiling area and the area of the wall at the eave edge that is above the EPS that guards the eave edge. The ceiling area is 96 in. by 76.25 in. (2.44 m by 1.94 m) and the exposed stub wall area is 96 in. by 2.5 in. (2.44 m by 0.064 m)—a total of 52.5 ft^2 (4.88 m^2). The exposed eave wall contributes only 3.2% to the total area.

Above the ceiling of the test section, triangular pieces of fiberglass batt insulation are seen in Figure lb on the ends of the attic formed by the trusses and the roof. The pieces are 1 ft (0.3 m) beyond the metering chamber. Their kraft paper facing ensures that they block the ends of the attic space and airflow along it, except that from natural convection currents inside. Polyethylene was stapled over the ends of the half trusses at the ridge edge to seal the attic from air leakage. Neither the fiberglass nor the polyethylene affect the heat transfer through the thin metal roof over the test section. The entire gypsum ceiling was covered by a piece of polyethylene air barrier/vapor retarder before the trusses were installed. It is assumed, therefore, that no air or moisture flowed between the climate and metering chambers during any of the tests.

Figure 2 introduces a naming convention for the three insulation configurations and shows a cross section of each one as it was installed inside the attic space between the 24-in. (0.61-m) o.c. nominal 2-in by 2-in. (actual 38-mm by 38-mm) ceiling joists. The fiberglass batts were a full 24 in. (0.61 m) wide and measured 2.25 in. (57 mm) in thickness when in place. Pieces were cut from rolls to the 82-in. (2.1-m) width from eave to ridge. Bulk density of two typical pieces was measured as 0.53 lb/ft^3 (8.5 kg/m^3). All the pieces were easily forced into the 22.5-in. (0.57-m) space between horizontal joists to form the first layer for all three configurations. Small air gaps occurred in all three where the upper 0.75 in. (1.9 cm) of the batts recover from the force fit. In the base-case configuration A, another layer of these batts was laid over the first layer in the same direction. Each piece was able to butt closely against its neighbors except where vertical and slanted truss members interfered. For ease of installation during the assembly of manufactured homes, a second layer of batts is not installed at right angles to the joists in order to reduce the effects of joists. When the metal roof was replaced, the two layers of configuration A were compressed up to 44% at the eave edge.

The PEPs that were used in configuration B were donated by a German manufacturer and compressed the

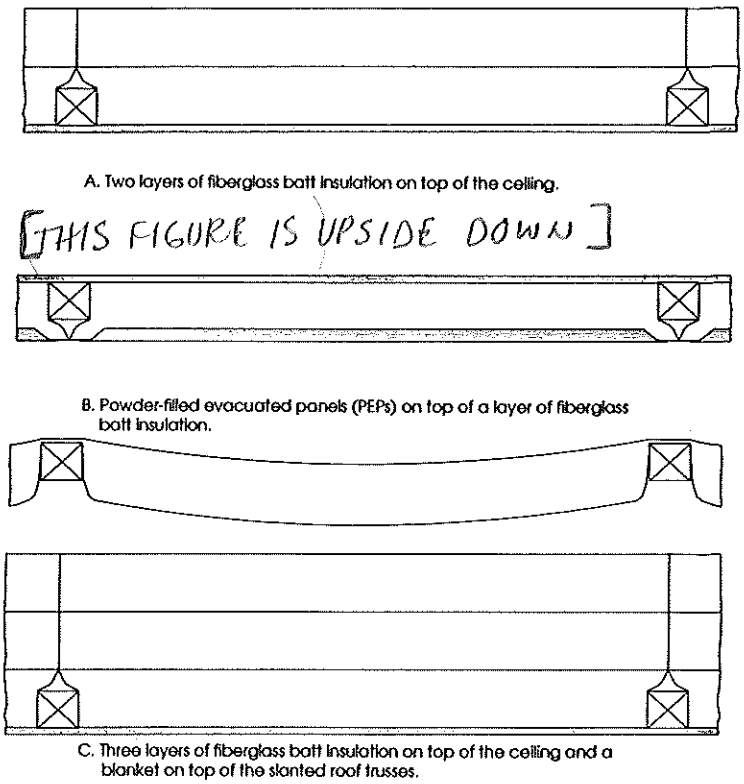

Figure 2 *Cross section of insulation configurations A, B, and C shown to scale between nominal 2×2 in. (actual 38×38 mm) horizontal ceiling joists 24 in. (0.61 m) o.c.*

layer of fiberglass batts on which they lay by about 0.125 in. (0.32 cm) everywhere. They were 0.79 in. (20 mm) thick and just narrow enough (about 22.5 in. [0.57 m]) to fit between the ceiling joists and trusses. The top of each panel shown in Figure 2 consisted of foil, such as heavy-duty household foil. A shallow plastic container held the silica powder that formed the body of the panel. The edges of the plastic container were sealed to the foil to form a band about 0.5 in. (1.3 cm) wide around the edge. The band was flexible enough that irregularities in truss spacing were accommodated by slight flexing. Figure 2b shows how the PEPs left underinsulated spaces over the joists, which can also be seen in the photograph in Figure lb, along with the gaps every 30 in. (0.76 m) because of the limited length of the PEPs. The length was such that the third panel in each space extended about 6 in. (15 cm) past the ridge edge. The polyethylene on the ridge edge was slit to allow the PEPs to rest in a slot cut out of the EPS guard insulation on the ridge edge.

For configuration C, three layers of the 24 in. (0.61 m) wide fiberglass batts were laid on the ceiling and a blanket from the same thickness of fiberglass was placed over the trusses. The pieces for the blanket were wide enough so there was only one taped splice in the whole blanket. When the metal roof was rolled over this blanket, the fiberglass was compressed by 89% over the trusses to a thickness of about 0.25 in. (6.4 mm). All four layers were

compressed up to 72% at the eave edge. Between trusses and away from the eave edge, the four batts are 9.0 in. (23 cm) thick if expanded to the same thickness as batts on the laboratory floor before installation and the first layer installed in the test section for all configurations.

The test section was equipped with a total of 97 copper-constantan thermocouples to supplement the thermocouples built into the upper and lower chambers of the LSCS for control and monitoring purposes. The thermocouples measured air and surface temperatures in the ceiling space, outside the test section, and inside the attic space. Eight provided temperature differences (ΔT) along the horizontal OSB extensions around the perimeter. Pairs were placed on the underside of the OSB on each of the four sides. On the eave side, the pair was Δx = 8.5 in. (22 cm) apart; on the ridge side, 25 in. (64 cm) apart; and, on the two ends, 13.5 in. (34 cm) apart. Both thermocouples of each pair were visible from the guard chamber. The gradients $\Delta T/\Delta x$ were multiplied by the thermal conductivity of OSB and by the cross-sectional area perpendicular to Δx to estimate the heat flow along each OSB extension into the metering chamber. The amounts were negligible compared to the measured total heat flow. Several temperatures were measured specifically to validate the model of the edge, which was done to provide details about the results of the tests. The ceiling and inside side-wall surfaces in the mid-plane of the test section were instrumented with thermocouples at the inside corner and at 1.5 in. and 3 in. (3.8 cm and 7.6 cm) from it both horizontally and vertically. Six thermocouples were located outside the test section on the aluminum siding at the level of and below the top plate. There were also two thermocouples inside the attic space at the edge where the perimeter rail and the top of the gypsum ceiling met. Averages were taken for the outside and attic edge temperatures. Thermocouples were also located to give temperature differences across the insulation throughout the attic. See Petrie et al. (1995) for specific locations of all the thermocouples.

Besides the three heat flux transducers (HFTs) calibrated facing XPS and used to estimate the flanking losses on the ridge wall and the end walls under the ceiling, three other HFTs were calibrated facing a specimen from the same roll of fiberglass batts as was used to insulate the test section. Two layers of the batts were cut in a 2-ft (0.66-m) square to fit in a heat flowmeter (ASTM 1991). After calibration, they were taped in place on the top of the ceiling in the middle truss space at selected distances out from the inside of the perimeter rail, a nominal 1-in. by 3-in. (actual 19-mm by 64-mm) wood board that was nailed to the ends of the trusses at the eave edge. At first, one HFT was placed with its edge against the perimeter rail, while the other two were placed at approximately 0.4 and 0.8 of the distance from the rail to the ridge along the top of the gypsum ceiling. The sensors at the 0.4 and 0.8 locations gave essentially identical results; the one against the perimeter rail yielded confusing data. Thermocouples inside and outside the perimeter rail near this HFT suggested a large temperature gradient along this HFT. HFTs are calibrated for one-dimensional heat flow across them so its calibration constant could not be used to determine the heat flux at the edge.

In the first three tests with the base-case insulation configuration, the HFTs at the 0.4 and 0.8 locations were covered by two batts of fiberglass, each expanded to a thickness of 2.25 in. (5.7 cm), which is given as the fully expanded thickness on the insulation package label. The nominal (at 75°F [24°C]) R-value of one batt is R_{US} - 7 (R_{SI} - 1.2) at a nominal thickness of 2.25 in. (5.7 cm). Figure 3 shows R-values of two layers of these fiberglass batts as a function of mean insulation temperature. The R-values using HFT data are computed from $\Delta T/q$, where ΔT is the temperature difference between thermocouples on top of the insulation and beside each HFT, and q is the measured heat flux. R-values from three tests at winter conditions and one test at summer conditions are plotted. Each mean temperature is the average of the temperatures used for the respective ΔT. The solid circle at 75°F (24°C) is the R-value of the specimen used for calibration of the HFTs. The solid line in Figure 3 is a correlation by Wilkes (1979) for the R-value of fiberglass batt insulation per unit area (A) as a function of temperature (T) with T_{nom} = 75°F (24°C) when thickness (L) = 4.5 in. (11.4 cm) and density (ρ_{nom}) = 0.624 lb/ft^3 (10.0 kg/m^3):

$$R = \frac{L}{kA} \text{ with } k_{nom} = 0.19815 + 0.001573 \cdot (\rho/\rho_{nom}) + 0.11686 \cdot (\rho_{nom}/\rho) \text{ and } k_T = k_{nom} \exp\,[0.0020201 + 0.0018486 \cdot (\rho_{nom}/\rho)\,(T - 75)]\,. \quad (1)$$

The thermal conductivity (k) in Equation 1 is in Btu in./(h·ft^2·°F) and temperature (T) is in °F. This correlation

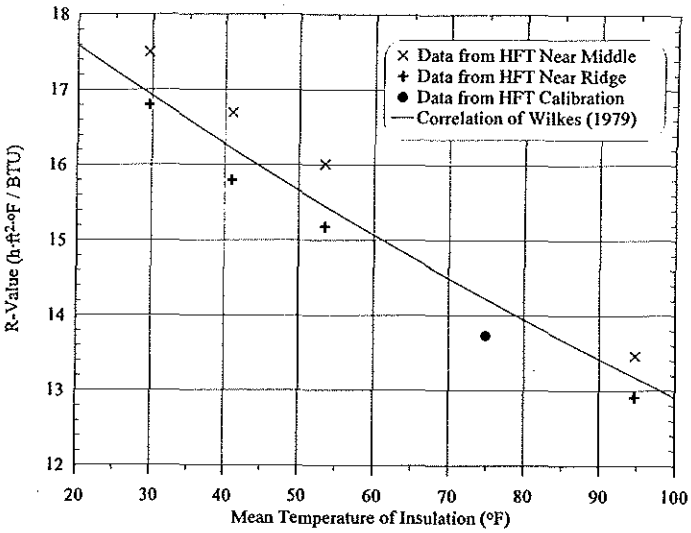

Figure 3 Center-of-cavity insulation R-values for configuration A.

is also used later in this paper to predict R-values for compressed fiberglass batts at selected temperatures. Note the difference between ρ_{nom} = 0.625 lb/ft^3 that is needed to fit the measured center-of-cavity R-values and $\rho_{measured}$ = 0.53 lb/ft^3 for the batts used in the tests. The apparent thermal conductivity of the fiberglass batts used in the tests was 0.32 Btu·in./(h·ft^2·°F) (0.046 W/[m^2·K]). This value yields a fiber diameter of about 20 × 10^{-5} in. (0.005 mm) at the measured density, rather than about 28 × 10^{-5} in. (0.007 mm) at the nominal density for Equation 1 (ASHRAE 1993b). The smaller fiber diameter is more typical of fiberglass batts produced currently and used in the tests; the larger fiber diameter is typical of fiberglass batts described in Wilkes' correlation (Wilkes 1995). The data from the HFTs at the 0.4 and 0.8 locations agree with the correlation to within ±0.4 h·ft^2·°F/Btu (±0.07 m^2·K/W), ±3% of the R-value, which corresponds to ±0.125 in. (±3.2 mm) uncertainty in the thickness of the fiberglass batts. This could easily be due to variations in the placement of the thermocouples on top of the batts. The point from the heat flowmeter apparatus lies within about the same error band. Figure 3 shows that the two HFTs and associated thermocouples give data for accurate center-of-cavity R-values with acceptable scatter of results from the individual HFTs.

For the rest of the tests, the HFT that was against the perimeter rail was moved away from the edge by 2.75 in. (7.0 cm) to a location just beyond the edge of the nominal 2-in. by 4-in. piece of wood that was laid flat over the top of the wall studs and formed the top plate. The HFT at the 0.4 location was moved to a location 10 in. (25 cm) beyond the first, that is, just beyond the end of the region in which the roof compressed the two layers of batt insulation used as the base case. The HFT at the 0.8 location was moved to the 0.4 location, where the attic space is more than 9.5 in. (24 cm) high and has room for four layers of batts expanded to the thickness observed for the first two layers.

TEST CONDITIONS

A listing of temperatures imposed in the tests is shown in Table 1. Designations for the tests use W1, W2, W3, or S2 for these conditions with an "A," "B," or "C" suffix to denote the insulation configuration. An "r" suffix is used for a repeated run at conditions and insulation

TABLE 1 **Temperatures Imposed in the Chambers of the LSCS for Tests with the Manufactured Home**

Winter	Climate Chamber	Metering and Guard Chambers
W1	25°F (–4°C)	75°F (24°C)
W2	0°F (–18°C)	75°F (24°C)
W3	–25°F (–32°C)	75°F (24°C)
Summer	**Climate Chamber**	**Metering and Guard Chambers**
S2	125°F (52°C)	75°F (24°C)

configuration identical to the unsuffixed one. An "x" suffix is for an extended run with some changes to the insulation configuration, such as additional sheathing. The randomized order of tests with the base-case insulation configuration was W2A, W1A, W3A, W1Ar, S2A, W2Ar, and S2Ar. The repetition W1Ar was done between W3A and S2A to check reproducibility. The locations of the HFTs under the attic insulation were then changed. W2Ar was done after S2A as a check before installing the PEPs. Test S2A was too short to achieve steady conditions because condensate was found at the bottom of the insulation during post-test inspection. Test S2Ar was done several months later as explained below. The order for the regular tests with the PEPs was W2B, W3B, W1B, and W1Br. The last two runs were done just before and immediately after the dead air spaces next to the OSB walls were filled with fiberglass batt insulation. These runs verified that less heat was flowing through the OSB walls after the spaces were insulated.

The extension of W2B, test W2Bx, was scheduled when configuration B did not improve system performance significantly. EPS blocks were sawed to an actual 4-in. by 4-in. (10-cm by 10-cm) cross section. Pieces were cut to fit between the vertical truss members and tapered to fit under the slanting truss members. Other lengths were cut to fit crosswise over the joints between PEPs. Strips of the R-7 fiberglass batts were placed under the EPS blocks and all joists and joints were covered. Pieces of 0.75 in. (19 mm) thick XPS sheathing were cut to cover the vertical edge of the test section at the eave under the aluminum siding and the top of the trusses from the eave edge to about 20 in. (51 cm) from it under the roof. After the extended run with the PEPs, the XPS sheathing under the aluminum siding at the edge and under the roof was removed and configuration C, comprising four layers of fiberglass batts, was installed. Tests designated W2C, W1C, W3C, S2C, and W2Cr were run without the vertical XPS sheathing over the eave edge, followed by test W2Cx with this sheathing. It took the system a week to settle at condition S2 and allow 24 hours of data to be obtained at steady conditions from all sensors. Local heat fluxes and temperature differences across the insulation yielded insulation R-value. To achieve steady-state at summer conditions required the use of cooling in the metering chamber, and problems with the cooling loop made the system R-value inaccurate for S2C. Test W2Cr followed the original S2C to check reproducibility after the summer conditions.

An improved cooling loop in the metering chamber was installed after test W2Cr. The manufactured home test section was removed from the LSCS and the calibration panel was installed. Checks for lack of systematic errors in the metering chamber energy balance were done at winter and summer conditions. The manufactured home test section was then reinstalled to get R-values for tests S2Cr and S2Ar.

RESULTS OF TESTS

Figure 4 compares all data obtained for the behavior of the two layers of fiberglass batts (configuration A), the single layer topped by PEPs (configuration B), and the four layers of fiberglass batts (configuration C). The averages of the data at each mean temperature in Figure 3 are assigned to the corresponding center-of-cavity R-values for two layers of fiberglass batts. They vary from R_{US} – 15.6 to 17.2 (R_{SI} – 2.7 to 3.0) in winter. The summer test yielded R_{US} – 13.2 (R_{SI} – 2.3). Center-of-cavity values for the PEPs on top of a fiberglass batt are R_{US} – 24.0 to 25.8 (R_{SI} – 4.2 to 4.5) and were obtained only at winter conditions. These center-of-cavity values are 50% higher than the values for the two layers of fiberglass. In other words, the PEPs used here, with a thickness of about 0.79 in. (20 mm), are thermally equivalent, away from all edges, to two layers of the fiberglass batts used here with a thickness of 4.5 in. (11.4 cm). The four layers of fiberglass show R_{US} – 30.4 to 31.7 (R_{SI} – 5.4 to 5.6) at winter conditions and R_{US} – 27.6 (R_{SI} – 4.9) at the summer conditions.

The energy balance on the metering chamber is used to generate a system R-value, defined as

$$R_{system} = \Delta T \cdot A/Q \qquad (2)$$

where

ΔT = the difference between the average air temperatures above and below the test section,

A = the inside surface area of the test section exposed to the metering chamber, and

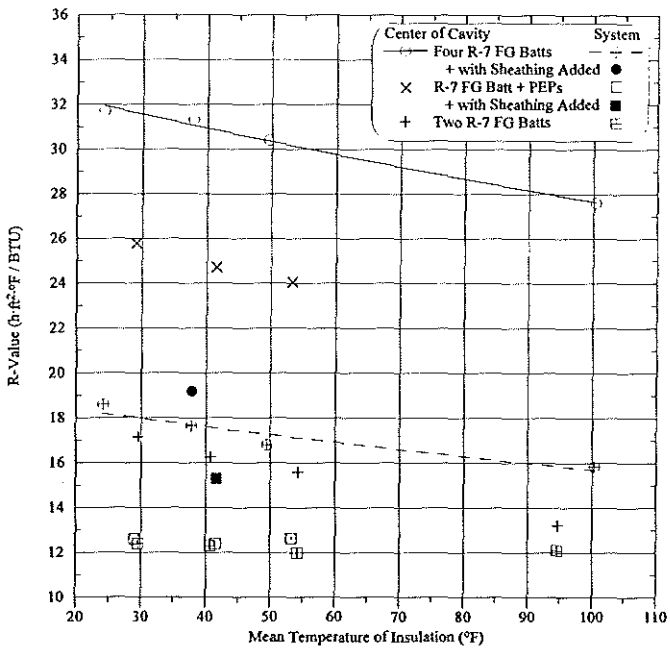

Figure 4 Comparison of the R-value across each of the three insulation configurations with its system R-value as a function of mean temperature.

Q = the net heat flow through this area after corrections for flanking losses around the perimeter of the test section.

As stated in the description of the test section, the area is the sum of the ceiling area and the area of the stub wall above the EPS on the eave side. It totals 52.5 ft² (4.89 m²), to which the exposed eave wall contributes only 3.2%.

The compression of insulation in the vertical direction at the eave edge with configurations A and C, the horizontal thermal bridge at the eave edge with all configurations, the underinsulation over the joists with configuration B, and the interference of vertical and slanted truss members with insulation coverage for all configurations contribute to a reduction of the system R-values below the center-of-cavity insulation R-values. Figure 4 documents its extent. For the base-case insulation (configuration A), the system R-values average R_{US} – 12.2 (R_{SI} – 2.1) and are 72% to 77% of the center-of-cavity R-values at winter conditions, rising to 92% at the summer conditions. Configuration B with PEPs shows a slight increase in system R-values to an average of 12.6, but they are only 49% to 53% of the higher center-of-cavity R-value for this configuration. The four layers of fiberglass batts (configuration C) achieve the best absolute performance, from R_{US} – 16.8 to 18.6 (R_{SI} – 3.0 to 3.3) at winter conditions and R_{US} – 15.9 (R_{SI} – 2.8) at the summer conditions, but this range is only 55% to 59% of the corresponding center-of-cavity R-values. Lines of best fit, assuming the inverse of the R-value is linear with temperature, are shown for the four fiberglass batts as a solid line through the center-of-cavity R-values and as a dashed line through the system R-values. There is more temperature dependence for the center-of-cavity R-values because they depend only on the properties of fiberglass, while the system values include non-temperature-dependent edge effects and effects of the vertical and slanted truss members. The system R-values for configuration B with PEPs show little temperature dependence because the edge and joist/joint effects are more pronounced.

If there are no systematic errors in the metering chamber energy balance, estimation of error reduces to consideration of random error. If the errors in the flanking losses are no more than ±10% of each loss, the random errors in the measured and corrected heat flows are the same. The 95% confidence interval for the corrected heat flow into the metering chamber and the system R-value around each one's average for the steady-state portion of each test can be estimated as the Student's test statistic multiplied by each one's standard deviation (Coleman and Steele 1989). Each portion yielded data that were recorded every 4 minutes for at least 12 hours of steady state. Thus, the Student's test statistic is 2 and the 95% confidence intervals are twice the standard deviations. Here the values are ±17 to 27 Btu/h (±60 to 90 W) for the corrected heat flows and ±0.5 h·ft²·°F/Btu (±0.09 m²·K/W) for the system R-values. The R-value for the PEP system in Figure 4 appears to be largest at the highest winter mean tempera-

ture, but the value is within the confidence interval about the average so the discrepancy is assigned to random error.

The center-of-cavity R-values for four fiberglass batts are 1.85 to 1.95 times the values for two layers, despite the effect of extra R-value from the air gap between the third layer and the blanket over the trusses. It is likely that the blanket over the trusses was not expanded between the trusses like the batts on the ceiling, but the roof prevented an actual measurement. Besides adding to the center-of-cavity R-value, the fourth layer of fiberglass batts provides a thermal break between the roof and the trusses. Thus, the significant improvement in system R-value is reasonable compared with what was achieved for two layers alone and for the PEPs on top of one layer. Moreover, the addition of 0.75 in. (19 mm) thick XPS sheathing (with nominal R_{US} – 3 or R_{SI} – 0.53) to the vertical edge at the eave produced an extra R_{US} – 1.6 (R_{SI} – 0.28) for the system and improved the system R-value by 9%. The value is shown as the solid circle in Figure 4.

The low ratio of system R-value to center-of-cavity R-value for the PEP system (49% to 53%) is a valuable lesson from these tests. Test W2Bx, parts 1 and 2, was done with extra sheathing to verify that the cause was effects at the eave edge and over the joists and joints. Test W2Bx1 had all sheathing in place, including the piece over the trusses near the eave edge. The system R-value improved to R_{US} – 15.3 (R_{SI} – 2.7), 23% better than the original R_{US} – 12.4 (R_{SI} – 2.2) from test W2B. This result is shown as the solid square in Figure 4. An additional part of this test, test W2Bx2, was done in which the sheathing over the trusses was removed. It showed that only 3.2% of the 23% improvement was due to the XPS sheathing over the trusses near the eave edge.

DISCUSSION OF RESULTS AND MODELING

Despite showing the lowest ratios of system R-value to center-of-cavity R-value among the three configurations, the one with PEPs provides high insulation value near the eave edge without significant compression of the insulation. The shaded bars in Figure 5 show edge R-values using data from the heat flux transducer centered 3.75 in. (9.5 cm) from the inside of the perimeter rail at the edge of the roof. It is just beyond the top plate, and total heat flux there is assumed to be indicated by the HFT. These edge R-values are compared with R-values across the uncompressed insulation in the center of the cavity from Figure 4. The latter form the unshaded upper bars in the figure. The early tests with the base-case insulation (configuration A at conditions W1 and W3) were conducted when the edge HFT was against the perimeter rail and it did not indicate the total heat flux. Data at the edge for configuration C were used to establish a slope vs. condition, which, along with the point for W2A, generated the two additional data for configuration A that are shown as shaded bars with dashed lines at the top of them.

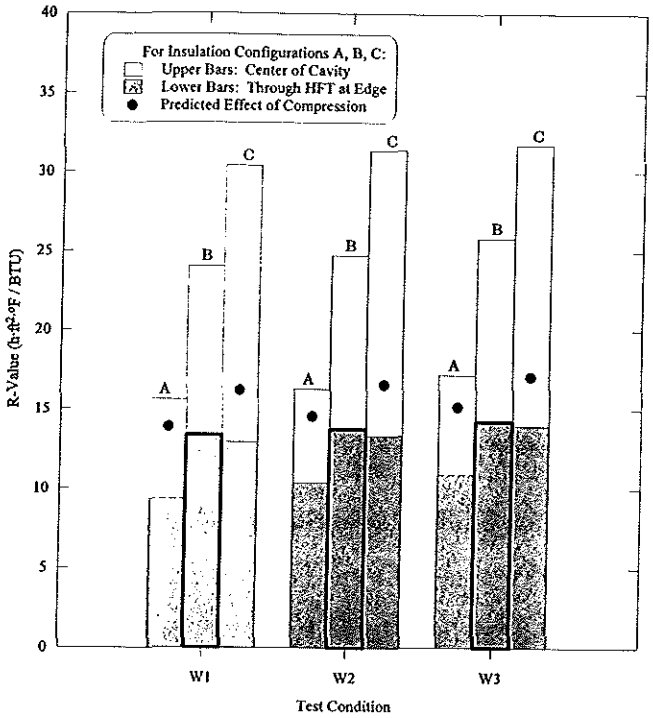

Figure 5 *R-values for insulation at the edge of the test section compared to center-of-cavity R-values.*

The trend for the center-of-cavity values going from configuration A to B to C is clearly different from the trend at the edge. The shaded and bolded bars for configuration B at the edge show higher R-values than do the shaded bars for either configuration A or C. The claim, based on the photograph in Figure 1a, is that configuration B with the PEPs causes no significant compression effects at the edge. The two layers in configuration A are compressed by 44% ($\rho/\rho_{nom} = 1.8$) at the very edge. There is 72% compression ($\rho/\rho_{nom} = 3.6$) at the very edge for configuration C. However, the effect of the horizontal thermal bridge remains with all configurations. For configurations A and C, the predicted effect of compression is shown by solid circles at each condition. These R-values are calculated from the thickness, density (which increases as thickness decreases due to compression), and average insulation temperature, using Equation 1.

Using procedures in ASTM C653-93 (ASTM 1992), we attempted to generate a curve of k_{nom} vs. ρ like that in Equation 1 specifically for the batts we used. In addition to k_{nom} itself, we measured $k/k_{nom} = 0.94$ compared to 0.96 from Equation 1 at $\rho/\rho_{nom} = 1.11$. Also, we measured $k/k_{nom} = 0.89$ vs. 0.93 at $\rho/\rho_{nom} = 1.25$. A curve like that in Equation 1 fit to the measured values did not extrapolate to reasonable k/k_{nom} at the high values of ρ/ρ_{nom} needed to predict the effect of compression of fiberglass batts at the edges.

Most of the differences between the center-of-cavity R-values and the R-values at the edge of the top plate for the highly compressed configuration C are explained by the effect of decreased thickness. The remaining amounts,

from the solid circles to the tops of the shaded bars, are due to the horizontal thermal bridge at the edge, which keeps the gypsum ceiling under the HFT at the edge cooler than the ceiling in the center of the cavity. Configuration A, which does not cover the trusses as well as configuration C, shows that more of the differences must be explained by the horizontal thermal bridge. All of the differences for configuration B must be explained by the horizontal thermal bridge. For this configuration, the eave edge is not filled with insulation. It is reasonable that configuration B shows the most decrease in R-value that must be explained by the horizontal thermal bridge.

Figure 5 shows that thermal performance at the eave edge is significantly worse than performance in the center of the cavity for all three insulation systems. Other causes for decreased thermal performance are lack of insulation coverage over ceiling joists and between panels with the PEPs as well as lack of insulation where vertical and slanted truss members penetrated all three insulation systems. To separate and evaluate the effects of each of these features, it is necessary to know each one's effect on the total measured heat flow into the metering chamber. Unfortunately, local measurements with an HFT at the details of interest are not reliable because of two- and three-dimensional effects.

We used a three-dimensional, transient heat conduction computer program (Childs 1993) to model a 24 in. (0.66 m) wide strip centered on a ceiling joist and applied it to the eave edge. The model of the edge went from the outside of the test section to a vertical plane 4.125 in. (10.5 cm) toward the ridge edge measured from the inside corner of the ceiling and to a horizontal plane down 7.5 in. (19.1 cm) from this comer. This region includes all heat flowing horizontally through the edge above the EPS guard insulation and vertically through the compressed fiberglass at the eave edge in the base-case configuration. The edge wall and ceiling surface area it includes is 8.4% of the assumed system area. The rectangular elements around the nodes in the model were chosen to reproduce the shape of the construction and insulation materials. Heat transfer coefficients at all boundary surfaces were specified. Boundary conditions were the measured air temperatures inside and outside the test section. The thermal properties of the construction and insulation materials were taken from the *1993 ASHRAE Handbook—Fundamentals* (ASHRAE 1993a), our center-of-cavity R-values, and Equation 1 for the effect of density and temperature on the R-values of fiberglass.

Four situations were used to check the model. Climate and metering chamber temperatures were those of condition W2. Thermal properties were inserted at an average temperature of 40°F (4°C). The tests modeled were W2A, W2B, and both parts of the extended test W2Bx. Combinations of reasonable values of the film heat transfer coefficient on the model of the inside ceiling and wall surfaces, the outside vertical edge, and the slanted roof edge were tried until the best agreement between measured and modeled temperatures was obtained. The best set of values was a heat transfer coefficient of 1.5 Btu/(h·ft^2·°F) (8.5 W/[m^2·K]) on the inside surfaces, a value of 0.5 Btu/(h·ft^2·°F) (2.8 W/[m^2·K]) on the outside wall, and 0.25 Btu/(h·ft^2·°F) (1.4 W/[m^2·K]) on the horizontal parts of the steps that modeled the slanted roof. The vertical parts of the model for the roof were assumed to be adiabatic. By "best" is meant that these heat transfer coefficients yielded temperatures on the inside and outside surfaces that were 2°F to 4°F (1°C to 2°C) above the respective measured values, but by the same amount for each case. Thus, the driving temperature differences between inside and outside surfaces were the same in the experiments and the models. The predicted attic edge temperatures varied from 1°F above to 3°F below the measured edge temperatures for the best values of heat transfer coefficients. This success with the modeling of temperatures is taken as evidence for accurate heat flow predictions with the model.

Heat transfer coefficients could not be specified exactly due to the uncertain flow patterns of air in the climate and metering chambers. Trials with 33% lower heat transfer coefficients on the inside surfaces and 100% higher ones on the outside yielded inside surface temperatures about 0.5°F closer to the measured values there. However, outside temperatures dropped to 2°F to 4°F below the measured values.

The model with thermal properties at the average insulation temperature of condition W2 and the best heat transfer coefficients was then applied to tests W1A, W3A, W1B, and W3B. The same goodness of agreement was achieved between predicted and measured temperatures. Table 2 lists the heat flow rates through the edge predicted by the model for all eight cases. The total measured flows from the metering chamber energy balance after corrections are also listed along with their 95% confidence intervals, the range of which was given above in the discussion of the system R-values shown in Figure 4. They average ±7.5% of the total heat flows in the table. The predicted heat flows through the edge are also assumed to be free of systematic errors and to have 95% confidence intervals that are ±7.5% of the smaller edge flows. The heat flow through the wall at the eave edge and 4.125 in. (10.5 cm) of the ceiling at the eave edge is 16.0% (within ±0.5%) of the total flow for all four cases at condition W2, although the area is only 8.4% of the system area. The ratios of predicted edge to measured total heat flow for the runs at conditions W1 and W3 are within ±0.5% of 16.0% except for test W1A. Measured heat flow for test W1A is +20 Btu/h higher than the heat flow for test W1B. This is inconsistent with the difference between W2A and W2B (+3 Btu/h) and between W3A and W3B (+5 Btu/h) but within the 95% confidence interval around the heat flow.

The predicted heat flows through the edge in column 2 of Table 2 were subtracted from the total heat flows in column 3. The results are values for $Q_{ceiling}$, the heat flow

TABLE 2 **Heat Flows for the Eave Edge and Whole Test Section and Resulting Data for the Ceiling Away from the Edge for Configurations A and B**

Test	Predicted Q_{edge} (Btu/h)	Measured $Q_{total} \pm u_Q$ (Btu/h)	Predicted $R_{ceiling}$ (h·ft²·°F/Btu)	Measured R_{center} (h·ft²·°F/Btu)	$FE_{ceiling}$
W1A	32.7	223 ± 23	12.4	15.6	0.21
W2A	48.9	314 ± 23	13 3	16.3	0.19
W3A	66.6	423 ± 25	13.5	17.2	0.21
W1B	33.1	203 ± 18	14.2	24.1	0.41
W2B	49.3	311 ± 22	13.5	24.7	0.45
W2Bx1	41.3	252 ± 18	16.7	24.7	0.32
W2Bx2	42.7	260 ± 17	16.2	24.7	0.34
W3B	67.3	418 ± 27	13.7	25.8	0.47

through the ceiling away from the edge. $Q_{ceiling}$ should not be affected significantly by edge effects but is affected by the ceiling joists, roof trusses, and, for the PEPs, joints between panels. A framing effect, $FE_{ceiling}$, is defined as

$$FE_{ceiling} = 1 - R_{ceiling}/R_{center} \quad (3)$$

where, by Equation 2, $R_{ceiling} = \Delta T \cdot A_{ceiling}/Q_{ceiling}$. Here $A_{ceiling} = 48.1$ ft²; it does not include the area of the ceiling included in the edge model. The temperature difference (ΔT) and R_{center} are available from the center-of-cavity data. $FE_{ceiling}$ displays how much the maximum R-value through the center-of-cavity insulation is reduced due to the effect of structural members and, in the case of PEPs, less R-value between panels and over the joists. Table 2 lists $R_{ceiling}$, R_{center}, and $FE_{ceiling}$ from Equation 3 for the tests with configurations A and B and both tests with configuration Bx.

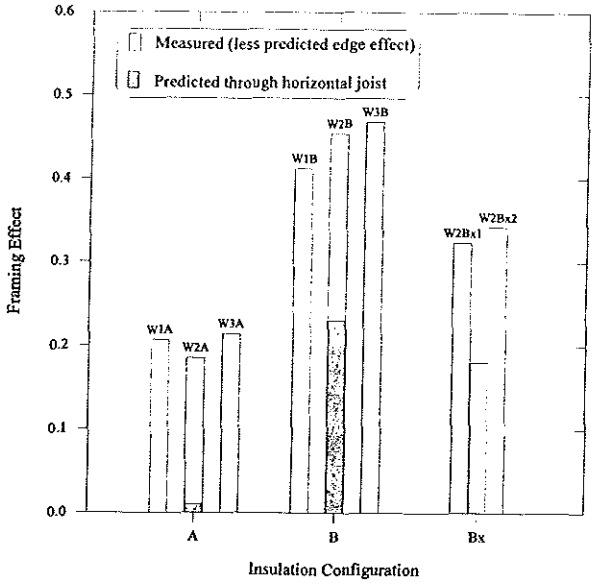

Figure 6 Comparisons of framing effects for insulation configurations A, B, and Bx.

For comparison to $FE_{ceiling}$, a model was also developed of a 24 in. (0.66 m) wide strip over a ceiling joist away from the edge and penetrations by vertical and slanted truss members. The base-case insulation configuration A, two layers of fiberglass batts, was modeled. At condition W2, the model predicted a framing effect of 0.01 vs. 0.19 to 0.21 for the ceiling value in Table 2 for tests W1A, W2A, and W3A, a difference of 0.18 to 0.20. Visual inspection of the gaps caused by the vertical and slanted truss members showed that the gaps extended for more than 60% of the length between the eave and the ridge.

Another run of the model for a horizontal joist was done for configuration B, PEPs on top of a layer of fiberglass batts. For this case, a dead air pocket was included above the joist to model the way that the joists prevented the tops of the batts from butting together (see Figure 2). The predicted framing effect was 0.23 compared to 0.41 to 0.47 in Table 2 for tests W1B, W2B, and W3B without the extra sheathing, a difference of 0.18 to 0.24.

To test the effect of the sheathing over the joists and joints between PEPs, a final run had 4-in. (10-cm) square blocks of EPS centered over the joists on top of the PEPs. It yielded a framing effect of 0.18 compared to 0.32 to 0.34 in Table 2 for tests W2Bxl and W2Bx2, a difference of 0.14 to 0.16. The comparisons between the predicted and ceiling framing effects are shown in Figure 6. The relatively high heat flow for test W1A that was demonstrated in Table 2 makes for a relatively small $R_{ceiling}$ and a relatively high framing effect for this case. The difference between the ceiling and predicted framing effects is the same within scatter for the A and B series of tests, which is consistent with a uniform effect of the vertical and slanted truss members. The difference is slightly smaller for the Bx cases, with sheathing over much of the joists and the joints between PEPs. Relative to the A and B tests, the Bx tests attempted to achieve uniform coverage by insulation and included sheathing tapered to fit under the slanted truss members. Effects of vertical members were not addressed. It is reasonable that the framing effects for the ceiling in the Bx tests came closer to the predictions of the model for them, which had no joints between PEPs, the same size of sheathing that was actually used to cover flaws, and no effect of vertical or slanted truss members.

CONCLUSIONS AND RECOMMENDATIONS

The system R-values for the three insulation configurations that were tested showed the effects of a horizontal thermal bridge at the edge of the roof caused by the construction features of the test section. The system with PEPs was not affected by compression of insulation at the eave but was by poor insulation coverage. Poor coverage occurred over the joists because the panels had to fit between the vertical and slanted truss members and over the joints

between the three panels used from eave to ridge in each space between joists. The other two configurations had compressed insulation at the eave, but insulation was continuous from eave to ridge. For all configurations, the full-width batts had to bend around the vertical and slanted truss members that connected to the ceiling joists.

The computer model of the eave edge for the base-case insulation package and for the superinsulation with PEPs showed that 16% of the total heat flow through the test section came through the eave edge. The model for the framing effects over the ceiling showed a joist effect of only 1% for the two layers of fiberglass batts but about 18% and 23% for the PEPs on top of a layer of fiberglass batts with and without sheathing, respectively. The differences between the joist and total ceiling framing effects were about 20% for the insulation configurations without extra sheathing, implying that the vertical and slanted truss members effectively reduced the system R-value from the center-of-cavity insulation R-value by about 20%.

The PEPs used in this study did not improve system R-values because of remaining edge effects and effects of poor insulation of the joists and joints between panels. PEPs can be recommended in this type of manufactured home only if a way is found to incorporate a continuous layer of this superinsulation in the roof cavity without danger of damage to it, perhaps by replacing the roof and trusses with a stress skin panel. The remaining effect of the horizontal thermal bridge at the edge can be lessened by using insulating sheathing on the side and end walls of manufactured homes.

REFERENCES

ASHRAE. 1993a. *1993 ASHRAE handbook—Fundamentals*, chaps. 22, 36. Atlanta: American Society of Heating, Refrigerating and Air-Conditioning Engineers, Inc.

ASHRAE. 1993b. *1993 ASHRAE handbook—Fundamentals*, chap. 20, Fig. 2. Atlanta: American Society of Heating, Refrigerating and Air-Conditioning Engineers, Inc.

ASTM. 1989. ASTM C236-89, Standard test method for steady-state performance of building assemblies by means of a guarded hot box, pp. 53-63, vol. 04.06, *Annual Book of Standards*. Philadelphia: American Society for Testing and Materials.

ASTM. 1991. ASTM C518-91, Standard test method for steady-state heat flux measurements and thermal transmission properties by means of the heat flow meter apparatus, pp. 153-164, vol. 04.06, *Annual Book of Standards*. Philadelphia: American Society for Testing and Materials.

ASTM. 1992. ASTM C653-92, Standard guide for determination of the thermal resistance of low-density mineral fiber insulation, pp. 251-255, vol. 04.06, *Annual Book of Standards*. Philadelphia: American Society for Testing and Materials.

Childs, K.W. 1993. Heating 7.2 users' manual. ORNL Report No. ORNL/TM-12262. Oak Ridge, Tenn.: Oak Ridge National Laboratory.

Coleman, H.W., and W.G. Steele. 1989. *Experimentation and uncertainty analysis for engineers*, chaps. 1-2. New York: J. Wiley and Sons.

Courville, G.E., P.H. Shipp, T.W. Petrie, and P.W. Childs. 1989. Comparison of the dynamic thermal performance of insulated roof systems. *Proceedings, 9th Conference on Roofing Technology*, pp. 50-55. Rosemount, Ill.: National Roofing Contractors Association.

Kosny, J., and J.E. Christian. 1995a. Comparison of thermal performance of wood stud and metal frame wall systems. *J. Thermal Insulation and Building Envelopes* 19: 59-71.

Kosny, J., and J.E. Christian. 1995b. Thermal evaluation of several configurations of insulation and structural materials for some metal stud walls. *Energy and Buildings* 22: 157-163.

Pederson, C. Rode, T.W. Petrie, G.E. Courville, A.O. Desjarlais, P.W. Childs, and K.E. Wilkes. 1992. Moisture effects in low-slope roofs: Drying rates after water addition with various vapor retarders. ORNL Report No. ORNL/CON-308. Oak Ridge, Tenn.: Oak Ridge National Laboratory.

Petrie, T.W., G.E. Courville, P.H. Shipp, and P.W. Childs. 1989. Measured R-values for two horizontal reflective cavities in series. *Thermal Performance of the Exterior Envelope of Buildings IV*, pp. 250-257. Atlanta: American Society of Heating, Refrigerating and Air-Conditioning Engineers, Inc.

Petrie, T.W., J. Kosny, and P.W. Childs. 1995. The evaluation of superinsulation to improve the energy efficiency of manufactured housing: Tests in the large scale climate simulator. ORNL Report No. ORNL/CON-407. Oak Ridge, Tenn.: Oak Ridge National Laboratory.

Wilkes, K.E. 1979. Thermophysical properties data base activities at Owens-Corning Fiberglas. *Proceedings of the 1979 ASHRAE/DOE-ORNL Conference on the Thermal Performance of the Exterior Envelope of Buildings*, pp. 662-677. Atlanta: American Society of Heating, Refrigerating and Air-Conditioning Engineers, Inc.

Wilkes, K.E. 1995. Private communication.

Wilkes, K.E., and P.W. Childs. 1992. Thermal performance of fiberglass and cellulose attic insulations. *Proceedings of the ASHRAE/DOE-ORNL Conference, Thermal Performance of the Exterior Envelopes of Buildings V*, pp. 357-367. Atlanta: American Society of Heating, Refrigerating and Air-Conditioning Engineers, Inc.

Wilkes, K.E., R.L. Wendt, A. Delmas, and P.W. Childs. 1991a. Attic testing at the roof research center—Initial results. *Proceedings of the Third International Symposium on Roofing Technology*, pp. 391-400. Rosemount, Ill.: National Roofing Contractors Association.

Wilkes, K.E., R.L. Wendt, A. Delmas, and P.W. Childs. 1991b. Thermal performance of one loose-fill fiberglass attic insulation. Insulation Materials: Testing and Applications, 2d vol., pp. 275-291, ASTM STP 1116, R.S. Graves and D.C. Wysocki, eds. Philadelphia: American Society for Testing and Materials.